NANO · MICRO small
www.small-journal.com

Reversible Conductive Inkjet Printing of Healable and Recyclable Electrodes on Cardboard and Paper

*Dong Jin Kang, Yvonne Jüttke, Lola González-García, Alberto Escudero, Marcel Haft, and Tobias Kraus**

Conductive inkjet printing with metal nanoparticles is irreversible because the particles are sintered into a continuous metal film. The resulting structures are difficult to remove or repair and prone to cracking. Here, a hybrid ink is used to obviate the sintering step and print interconnected particle networks that become highly conductive immediately after drying. It is shown that reversible conductive printing is possible on low-cost cardboard samples after applying standard paper industry coats that are adapted in terms of surface energy and porosity. The conductivity of the printed films approaches that of sintered standard inks on the same substrate, but the mobility of the hybrid particle film makes them less sensitive to cracks during bending and folding of the substrate. Damages that occur can be partially repaired by wetting the film such that particle mobility is increased and particles move to bridge insulating gaps in the film. It is demonstrated that the conductive material can be recovered from the cardboard at the end of its life time and be redispersed to recycle the particles and reuse them in conductive inks.

Paper and cardboard are lightweight, renewable materials with a large recycling rate (85% in Europe[1], 64.7% in the USA[2]) that constitute an interesting alternative to artificial polymers. Cardboard dominates the packaging industry today and is likely to increase its share in the future.[3] The use of cardboard as part of long-lived customer goods has been increasing in the last two decades; today, products include cardboard furniture and wallpaper with temperature, climate, and humidity regulating functions.[4] It is possible to deep-draw paper-based materials and replace molded parts in vehicle construction[5,6] with lightweight structures that can be recycled.

The integration of electrical circuits directly in such parts would further increase their value. Printing on paper is a highly available, efficient process to add functionality in paper-based products.[7–10] Graphical printing on cardboard is widely applied in packaging; it retains the recyclability and properties of the base material. Functional printing can introduce electrical conductivity and other functions[11–14], but the resulting products are not foldable and hard to recycle. Commercially available inks contain metal nanoparticles (MNPs)—in most cases based on silver.[15–17] MNPs provide high electrical conductivity, versatility, and reproducibility compared to carbon materials and conducting polymers, whose electrical conductivity (normally 10 to 10^2 S cm^{-1}) is two to four orders of magnitude lower than that of metals.[18–20] The particles need to be sintered, however, which limits the choice of substrate since it must sustain the temperatures necessary for thermal sintering[21–23] (typically >250 °C) or enable chemical sintering, which requires chemical agents or specialty papers with polymer layers.[24–26] The *irreversible* sintering step immobilizes the metal and makes it difficult to recover it during recycling.[27] The resulting metal film is prone to cracking when the substrate is folded.[28,29]

In this contribution, we demonstrate the *reversible* functional inkjet printing of conductive structures using hybrid inks on cardboard substrates. Our material retains the integrity of the individual metal particles such that they can be recovered during recycling. We investigate how to lend the particles sufficient mobility such that they can reconfigure and thus repair cracks in the conductive structure. We study how to ensure sufficient adhesion and density of the printed structures to create stable conductive features.

Three key aspects are studied in the following. First, hybrid particles with a metal core and a conductive polymer shell are introduced to inkjet printing on paper for the first time. These particles can form conductive layers without a sintering step and form reversible conductive films simply by drying. Second, conventional paper is modified using systematic variants of traditional paper coats based on $CaCO_3$ and $CaSiO_3$ in order to obtain dense, conductive, adherent films of the hybrid inks. The coats modify the porosity and surface energy

Dr. D. J. Kang, Dr. L. González-García, Dr. A. Escudero, Prof. T. Kraus
INM – Leibniz Institute for New Materials
Campus D2 2, Saarbrücken 66123, Germany
E-mail: tobias.kraus@leibniz-inm.de
Dr. Y. Jüttke, Dr. M. Haft
PTS – Papiertechnische Stiftung
Pirnaer Straße 37, Heidenau 01809, Germany
Prof. T. Kraus
Colloid and Interface Chemistry
Saarland University
Saarbrücken 66123, Germany
The ORCID identification number(s) for the author(s) of this article can be found under https://doi.org/10.1002/smll.202000928.

DOI: 10.1002/smll.202000928

of the cardboard[30–32] and no further surface treatment is required for their use. Third, the reversibility is tested in order to repair conductive leads after bending and to recover the ink from irreparably damaged structures as illustrated in **Scheme 1**.

Our results show that hybrid inks can be combined with coated cardboard substrates to rapidly print conductive structures without any sintering. The adapted coat provides a combination of imbuing and drying that leads to a continuous, adhesive conductive film. It reduces the amount of ink required to print sufficiently conductive structures. Finally, we demonstrate the recovery of the metal particles from the paper through delamination and sonication.

We previously reported on sinter-free electronic inks that combine a gold nanoparticle core with a conductive polymer shell. A new ink was developed based on the same concept and adapted to printing on paper and cardboard.[33] First, gold nanoparticles (AuNPs) were synthetized using cetyl trimethylammonium bromide (CTAB) as surfactant and stabilizer. A route based on well-established protocols developed for the synthesis of gold rods provided quasi-spherical AuNPs with core diameters of 55 ± 21 nm (mean ± standard deviation). The core was then coated with a conjugated polymer, poly(3,4-ethylenedioxythiophene):polystyrene sulfonate (PEDOT:PSS) following a previously described ligand exchange protocol.[33] (The resistivity of pristine PEDOT:PSS is 3 ± 1 Ω cm for a 30–50 nm thick layer at room temperature.) The resulting hybrid particles were isolated, purified, and formulated as stable ink (**Figure 1**a and Figure S1, Supporting Information). Transmission electron microscopy (TEM) indicated a 1 nm layer of PEDOT:PSS around the gold core. This shell has a high electron density, and the π–π stacking of the polythiophene chains enables electron transfer between AuNPs when they touch upon drying.

The hybrid inkjet inks were water-based without additives and had a surface tension of $\gamma = 47 \pm 5$ mN m^{-1}, a viscosity $\eta = 7$ mPa s, a density of $\rho = 1.33 \pm 0.23$ g cm^{-3}, and a solid content of 200 mg mL^{-1}. The inkjet printer ejected droplets from nozzles with diameters of $d = 21$ µm at a speed of $v = 6.8 \pm 0.3$ m s^{-1} that we optimized as shown in Figure 1e and Figure S2 in the Supporting Information. A useful indication of printability is the inverse of the Ohnesorge number $\mathrm{Oh} = \eta/(v\rho d)^{1/2}$, often denoted Z, defined as the ratio of the Reynolds number $(\mathrm{Re}) = v\rho d/\eta$ and the square root of the Weber number $(\mathrm{We}) = v^2\rho d/\gamma$.[34] Our ink, which had $Z \approx 7$, formed stable and separated droplets without satellites as shown in Figure 1g. We prepared samples by direct-inkjet printing on a commercial photo paper (HP Glossy, 160 µm thick) and found resistivities in the range of 2.4–4.3 × 10^{-3} Ω cm immediately after drying (see Figure S3 and Video S1, Supporting Information).

The porosity and surface energy of the substrate are known to affect the spreading of the ink and the conductivity of the resulting layers as reported by Hsieh et al.[35] and others.[36,37] Printing on uncoated, highly porous cardboard did lead to relatively high resistivity of ≈8.3 × 10^{-1} Ω cm at 1 µm thickness

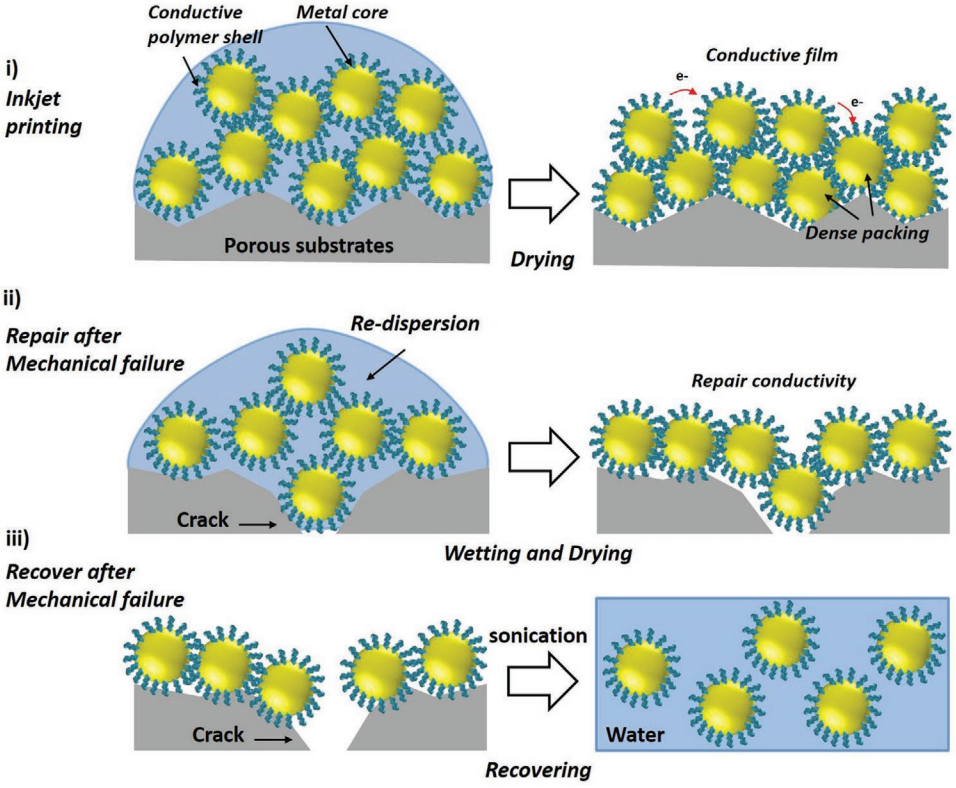

Scheme 1. Reversible inkjet printing of conductive structures on cardboard. i) Hybrid ink dries and forms a conductive film of densely packed particles that retain their identity. ii) The particles can be mobilized by wetting them, e.g., to repair cracks. iii) Recovery is possible for recycling by ultrasonic agitation; the particles can be reused for making ink.

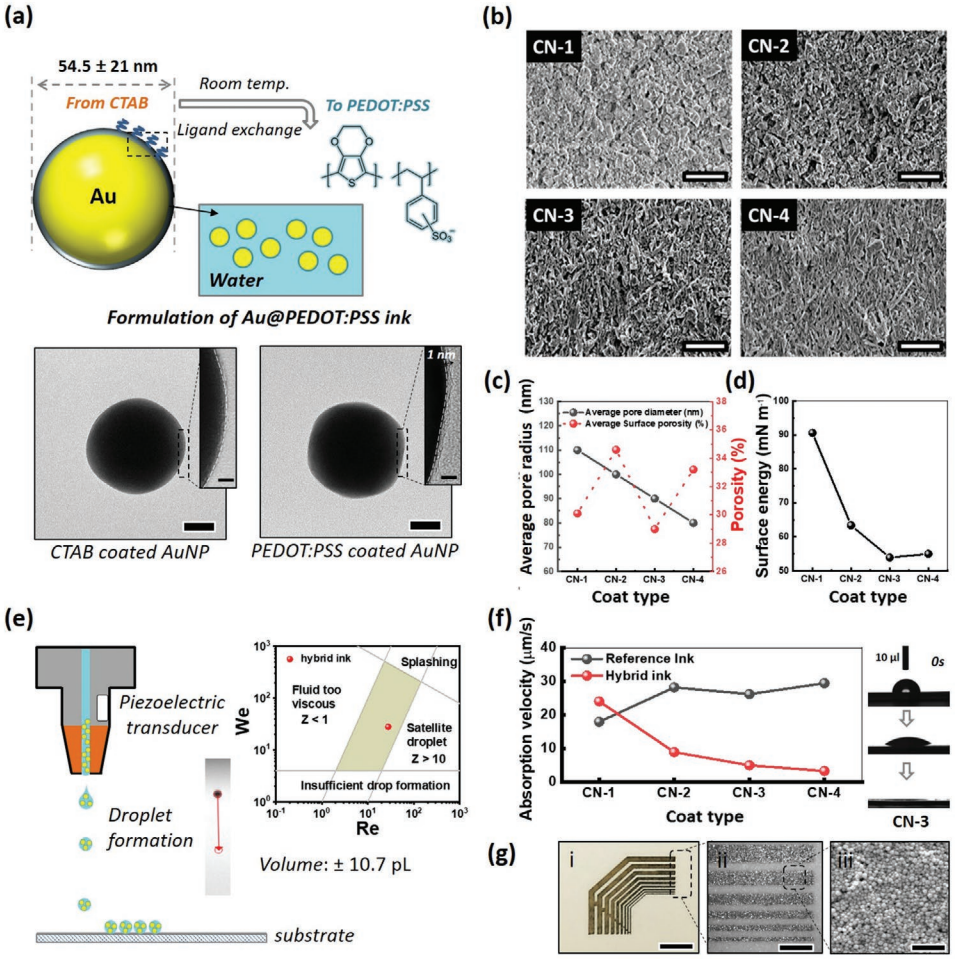

Figure 1. Inkjet printing of sinter-free Au ink on coated cardboards. a) Schematic illustration of PEDOT:PSS-coated AuNPs and TEM images before and after the ligand exchange. The scale bar is 20 and 2 nm (inset). b) Scanning electron micrographs of four different coating types on cardboard. The scale bar is 5 μm. c) Average pore radius (left) and porosity (right) of coated cardboards. d) Surface energy of coated cardboards. e) Schematic illustration of drop-on-demand piezoelectric inkjet printer for printing of sinter-free Au ink and a parameter map of the Re and We numbers for hybrid ink. Note that all formulations were in the range that is suitable for printing. f) Absorption velocity of reference ink and sinter-free Au ink on different coated cardboards and optical photographs of absorption behaviors of hybrid ink on coat CN-3. g) i) Photograph, ii) optical micrograph, and iii) scanning electron micrograph of an inkjet-printed conductive structure. The scale bars are 4 mm, 500 μm, and 500 nm.

of the printed electrode (Figure S4, Supporting Information). The standard way to reduce surface porosity in paper industry is coats based on aqueous dispersions of $CaCO_3$ and $CaSiO_3$. We used a mixture of natural and precipitated $CaCO_3$ pigment modified calcium carbonate (MCC), a $CaSiO_3$ pigment, and polyvinyl alcohol as binder, at a coating weight of 30 g m^{-2}. Four mixtures of these additives with different mass ratios of $CaCO_3$: $CaSiO_3$ (CN-1: 100:0, CN-2: 90:10, CN-3: 60:40, and CN-4: 30:70) were prepared and used to coat a commercial raw cardboard that is widely used as a packaging material (see Table S1 in the Supporting Information and experimental details below). Figure 1b shows scanning electron microscopy (SEM) images of the surface morphology of the four different coats. Increasing the fraction of flake-like $CaCO_3$ particles over the rod-shaped $CaSiO_3$ reduced the average pore radius, while the overall porosity hardly changed (Figure 1c). The surface energy gradually dropped with $CaSiO_3$ content due to the hydrophobic groups on the surface as shown in Figure 1d.[38]

Figure 1f shows the absorption rate of our hybrid NP ink as compared to a particle-free reference ink that only contained PEDOT:PSS. Reducing pore size and surface energy slightly increased the absorption rate of the reference ink but considerably decreased it for the hybrid NP ink. SEM images (Figure 2b and Figure S5, Supporting Information) suggested that this difference is due to the hybrid particles' accumulation on top of small pores. Hybrid inks formed a relatively dense particle layer on top of the substrate that strongly adhered due to its extension into the pores, similar to results obtained for standard metal inks previously.[37] Porous substrates are known to absorb the liquid rapidly, thus reducing the impact of evaporation and the accumulation of particles at the three-phase boundary line that leads to the so-called "coffee rings."[36]

Figure 2a shows the mean resistivity of structures printed on cardboard samples with different coats. We inkjet-printed strips of 2 cm × 0.3 cm using drop densities of 1000 to 2500 dpi and calculated specific resistivity (ρ) as resistance (R) × cross-sectional

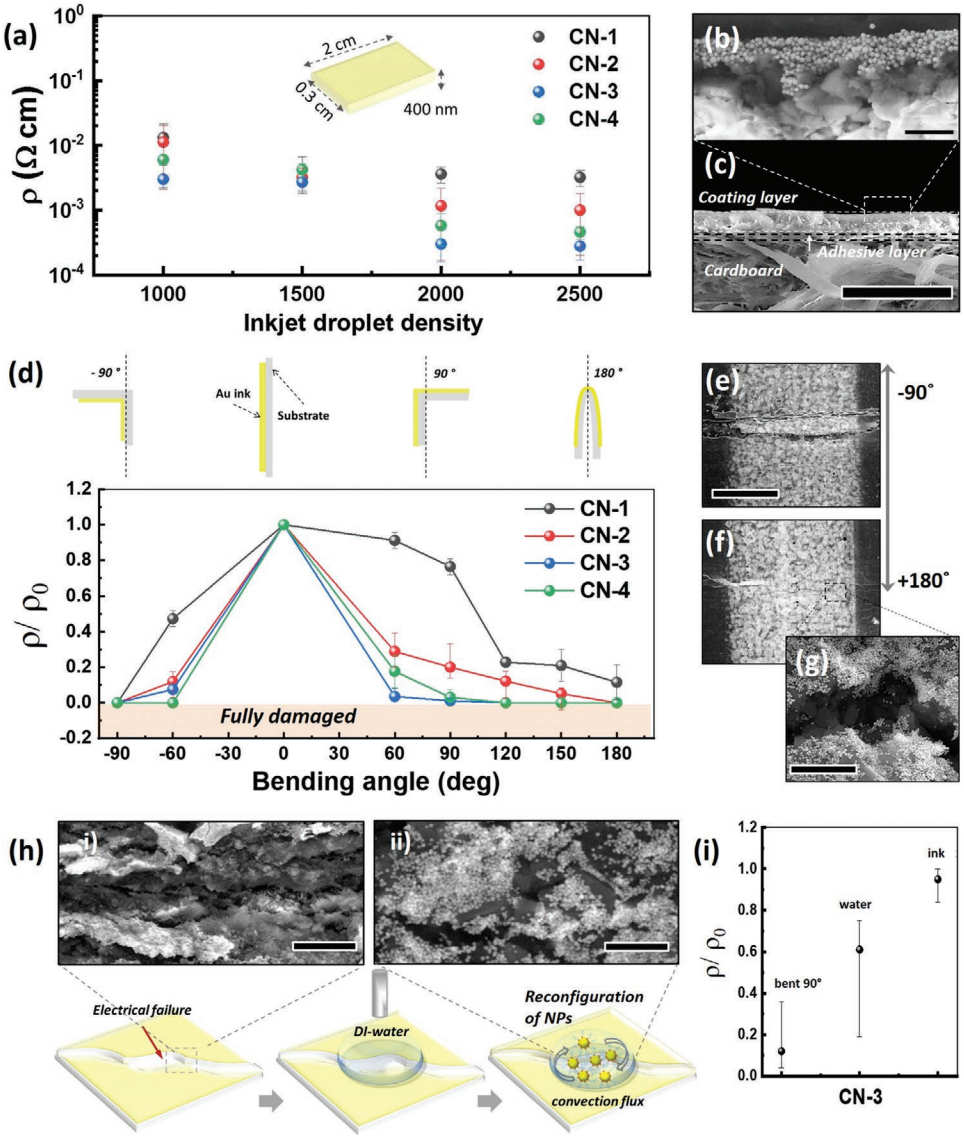

Figure 2. Electrical conductivity of inkjet-printed structures on coated cardboard. a) Specific resistivity as function of droplet density. b) Cross-sectional morphology of printed sinter-free Au ink on coating layer. The scale bar is 500 nm, c) Cross-sectional morphology of the printed particle film on coated cardboard (scale is 100 µm). d) Normalized resistivity after bending to angles from –90° to 180°. e) Scanning electron micrographs of the damages caused bending to –90° and f) 180° (scale bars are 500 µm) and g) detail of crack formed at 180° (scale bar is 2 µm). h) Mobilization of the particles by wetting to bridge the gap (scale bars are 10 and 1 µm). i) Normalized resistivity of the bent sample before and after treatment with water and ink.

area (A)/length of structure (l). Uncoated cardboard led to high resistivity on the order of ≈8.3×10^{-1} Ω cm even at 4000 dpi (thickness of layer = ≈1 µm). Microstructure analysis confirmed that the electrical conductivity was severely limited by the disconnected structure that the hybrid ink particles formed on the highly porous fiber structure of the uncoated cardboard (Figure S4, Supporting Information). The initial resistivity of coated cardboard was much lower and increased following the order CN-1 > CN-2 > CN-4 ≥ CN-3. Apparently, the low-porosity coatings and low surface energy of CN-3 and CN-4 decreased specific resistivity even at low drop densities.

Slow absorption and low surface energies led to smaller sessile droplets and increased the thickness, and possible the packing density, of the conductive film. This decreased resistivity. We found that the diameter of the printed dots (dried droplets) was larger on CN-1 (39.2 ± 2.8 µm) and CN-2 (36.1 ± 2.1 µm) than on CN-3 (35.7 ± 1.8 µm) and CN-4 (35.5 ± 1.3 µm) such that the areal density of particles was greatest for CN-3 (Figure S6, Supporting Information). A conceivable alternative mechanism that could lead to increased electrical performance when printing on small pores is the decrease of particles that are "lost" inside the bulk and do not contribute to electrical conduction (the extreme case of particle loss is the uncoated cardboard in Figure S4 in the Supporting Information). We did not find evidence for this mechanism for any of our coats, however. Cross-sectional electron micrographs of all printed films on coated cardboards indicate for all cases that, although the average pore size is larger than the particle

average diameter, only few particles migrated into the porous structure. Figure 2b and Figure S6 in the Supporting Information illustrate that the hybrid particles on all coats formed a continuous dense film on top.

The resistivity of the resulting films ($\rho \approx 5.2 \pm 0.4 \times 10^{-3}$ Ω cm) was slightly above that of sintered metal films printed with commercial inkjet inks on the same coated cardboards ($\rho \approx 7.8 \pm 1.3 \times 10^{-4}$ Ω cm) at 2000 dpi, but it is formed of individual particles that can be redispersed in liquid. In the following, we test two potential benefits of this reversibility: the repair of damages that occur when paper is bent and folded, and the recovery of the particles from the printed film at the end of device life time.

Folding is a versatile and common process in the production of packaging and other 3D structures from paper and cardboard. It would be highly desirable to fold conductive structures without reducing their performance. This is known to be difficult, however: folding of coated paper and cardboard leads to microscopic cracks that interrupt the conductive film.[39,40] In our study, conductive structures (2 cm long × 0.3 cm wide) were printed at 1500 dpi and bent to angles from −90° to +180°. Figure 2d shows the normalized resistivity (ρ/ρ_0) for the different coats and bending angles. The resistivity of all samples increased abruptly when bending to angles of 60° or above due to crack formation that was visible in SEM (Figure 2e,f). The analysis revealed a larger damaged area of the conductive film when bending to −90° than to 180°. This is consistent with previous reports of greater damage in printed conductive structures for compression than tension.[41] The drop in conductivity was always caused by the formation of cracks in the coats that propagated through the conductive layer and disconnected the particles in the hybrid particle layer. Some of the particles migrated into the crack (Figure 2g and Figure S8, Supporting Information), but their density was insufficient to electrically bridge the gap. It is interesting to note that CN-1 and CN-2 coats led to a greater bending stability than CN-3 and CN-4 although the latter two had a positive effect on the initial resistivity of the film (vide supra). Careful analyses of the micrographs and elastic moduli suggest that the larger fraction of $CaSiO_3$ in the coat makes them more brittle (Table S1, Supporting Information). We repeated the experiments with commercial silver nanoparticle (AgNP) inks (PV nanocell, Sicrys I50T-13) on the same substrates, sintered them (150 °C for 1 h), and analyzed the cracking of the sintered films on five samples each. Figure S7 in the Supporting Information indicates the formation of similar cracks at lower bending angles than for the unsintered hybrid ink samples above. The sintering process is likely to change the properties of coats, thus increasing their propensity for brittle cracking. The abrasion resistance of printed hybrid ink on cardboard substrates was evaluated using standard abrasion testing (ASTM D3884) that indicated good adhesion and sufficient yield strength to withstand removal. Conductivity was retained even after 500 strokes (Figure S9, Supporting Information).

We tested whether it is possible to increase the mobility of the hybrid particles in order to heal the cracks in the bent samples. A volume of 10 µL of deionized (DI) water was drop-coated over the entire damaged areas as shown in Figure 2h. The resistivity of the damaged electrodes recovered to up to 58% of their initial resistivity in 10 min after drying. A part of the particles was redispersed and filled the crack, thus re-establishing electrical contact. More effective than simple wetting was to repair the cracks with 10 µL of sinter-free Au ink, which leads to a recovery of 98% of its initial resistivity (Figure 2i).

We exploited the reversibility of the process in order to recover the hybrid particles from a printed structure.[42] The coat with the conductive structure can be mechanically peeled off the cardboard that is then suitable for standard paper recycling routes[43,44] and the recovery of the hybrid particles (**Figure 3**a,b). An ultrasonic bath (Elmasonic X-tra 50 H, frequency: 35 kHz) was used to agitate the peeled top layer in water for 5 min at room temperature (Figure 3c). Agglomerates

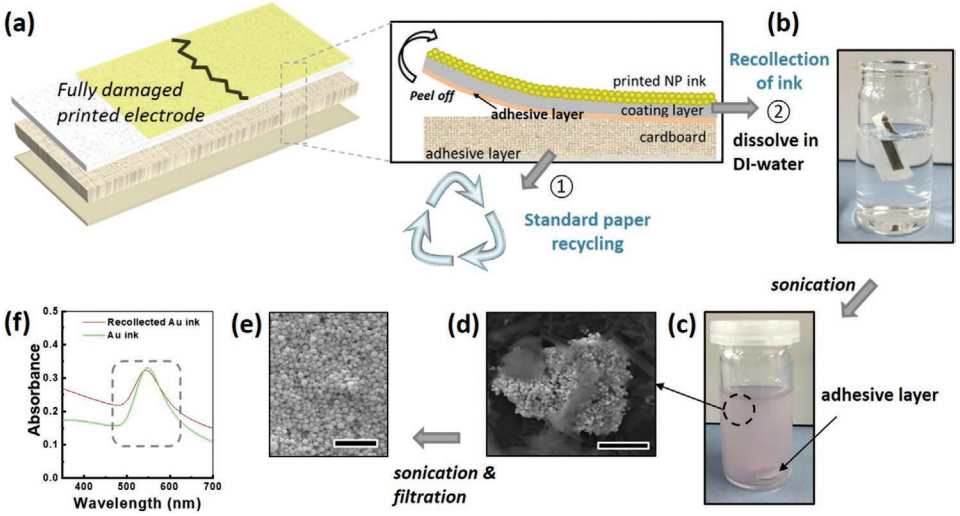

Figure 3. Recovery of hybrid nanoparticles from damaged electrodes. a) Schematic sample structure and separation of the coated layer from the cardboard base. b) Damaged top layer in water. c) Redispersion of hybrid particles by ultrasonication. d) Electron micrographs of recovered particle agglomerates (scale bar is 5 µm) before and e) after purification (scale bar is 500 nm). f) Optical transmission spectra of the original hybrid ink and recovered hybrid ink.

of the coating material mixed with sinter-free AuNPs were dispersed in DI water, further sonicated, and possible larger particles were removed using 0.2 and 0.45 µm membrane filters. The final dispersion was again ultrasonicated for 20 min at room temperature. A combination of SEM and UV-vis spectrometry shown in Figure 3d–f indicated that individual hybrid particles were successfully recollected at a recovery rate of ≈30% (see the Experimental Section for the detailed evaluation). We believe that this yield can be considerably increased using improved separation processes, e.g., the combination of mechanical and chemical treatment with ultrasonication processes.[45]

In summary, the reversible printing of sinter-free hybrid inks on cardboard yielded highly conductive, bendable electrodes that can be repaired and recycled. Tailored cardboard coats led to excellent conductivity of $\approx 5.2 \pm 0.4 \times 10^{-3}$ Ω cm without sintering that are comparable to those of sintered commercial Ag ink ($\approx 7.8 \pm 1.3 \times 10^{-4}$ Ω cm). The particles in the films retained their individual structure and could be mobilized on demand in order to repair cracks from bending or folding or to recover them from the devices, e.g., at the end of the life cycle. The hybrid ink concept is not limited to the gold particles used here and can be extended to metal cores of Ag, Cu, and other metals and semiconductors. We believe that it provides useful alternative routes to printed flexible electronic devices, RFID tags, and biosensors on paper and cardboard.

Experimental Section

Synthesis of AuNP@PEDOT:PSS Ink: A modification of the published synthesis of gold nanorod-based hybrid inks described in ref. [46] was employed for the synthesis of spherical AuNPs capped by CTAB (for synthesis, Sigma Aldrich). The gold content of the solution was increased in order to increase the yield per batch and the dispersion was ensured by vigorous stirring. In a second step, the ligand exchange procedure described in the previous work[33] was used to obtain hybrid AuNP@PEDOT:PSS nanoparticles dispersed in water. The concentration was adapted to 200 mg mL^{-1} solid content to prepare an ink with a surface tension of 47 ± 5 mN m^{-1}, a viscosity of 7 mPa s, and a density of 1.33 ± 0.23 g cm^{-3}. All reagents were used without further purification.

Preparation of Coated Cardboards: Pigments, binders, and additives were formulated to obtain applicable dispersions and applied on the raw commercial cardboard (Storaenso Tambrite with a basis weight of 250 g m^{-2}) to obtain a dried weight of 30 g m^{-2}. The dispersion contained a mixture of natural and precipitated $CaCO_3$ pigments MCC, a $CaSiO_3$ pigment, and polyvinyl alcohol (Mowiol 4–98) as binder; it showed no foam formation or settling. The mass ratio of MCC and $CaSiO_3$ pigments was varied. It was sometimes necessary to add a thickener in order to reach the necessary viscosity of 800 mPa s. All cardboard substrates were used without heat treatments.

Inkjet Printing of Hybrid Inks: Hybrid ink (200 mg mL^{-1} in water) was printed using a PiXDRO LP50 printer equipped with a piezo-type printhead comprising 21 µm diameter nozzles at room temperature (25 ± 3 °C). The jetting wave form was optimized as shown in Figure S3 in the Supporting Information. Specimens for electrical characterization were prepared on different cardboard pieces with 3 cm × 1 cm size.

Inkjet Printing of Conventional Inks: Commercial inks based on Ag (Sicrys I50T-13, PV nanocell, Israel) were printed on cardboards using a PiXDRO LP50 printer equipped with a 21 µm diameter inkjet nozzle at room temperature (25 ± 3 °C). Silver electrodes (thickness ≈3.3 µm) were sintered at 150 °C for 1 h after printing, as advised by the ink manufacturer.

Characterization of Printed Structures: An Infinite Focus IFM G3 microscope (Alicona GmbH, Germany) was used to quantify the surface roughness. It acquired an image stack by changing the focal plane on an area of 1.02 mm × 0.82 mm and calculated the roughness via image analysis. The Pore Master 60 GT mercury porosimeter from Quantachrome (now 3P instruments) was used to quantify pore radius and porosity. A capillary with the sample was evacuated in the device and filled with elemental mercury. The volume of mercury that entered the sample was measured continuously and the porosity of the substrate was subtracted. Surface energy was calculated using the standard characterization method developed by PTS (PTS-PP:103/85)[47] based on the geometric-mean equation.[48] Surface characteristics were obtained with a camera-based OCA 20 (Dataphysics, Germany) contact angle setup using 5 pL droplets of water and formamide, respectively. The viscosity of the hybrid ink was measured on a Discovery Hybrid Rheometer (HR-3, TA Instruments). Optical microscopy images were performed on a Zeiss Polscope Observer; SEM was performed with a Quanta 400 SEM at 10 kV acceleration voltage with a secondary electron detector (FEI, Germany). Transmission electron micrographs were recorded using a JEM 2010 at 200 kV accelerating voltage (JEOL, Germany). An abrasion test was performed following ASTM D3884 on ten CN-3 and CN-4 substrates with printed conductive lines of 5 × 1 cm using a force of 5 N and the same coated papers as counter pieces. A Keithley 2450 electrometer was employed for the electrical resistivity using current density–voltage characterizations with the four-probe method. All samples were flatted after bending and before the resistivity measurements and all the measurements were repeated five times with different samples for each experiment. Optical transmission spectra were obtained with a Cary 5000 UV-Vis–NIR Spectrophotometer. The recovery yield of the hybrid particles was estimated after recollection from 20 samples with dimensions of 2 cm (l) × 0.3 cm (w) × 400 nm (thickness) assuming an original mass fraction of hybrid particles of 0.28 w/w.

Supporting Information

Supporting Information is available from the Wiley Online Library or from the author.

Acknowledgements

The authors are grateful for financial support of this work in the form of an IGF project grant 19957 BG "IGLU." The authors thank Mr. Robert Strahl for preparation of the video about inkjet printing and Mr. Long Zhang for discussion about electrical measurements.

Conflict of Interest

The authors declare no conflict of interest.

Keywords

conductive inkjet printing, hybrid inks, metal nanoparticles, printed electronics, recycling, sustainable electronics

Received: February 13, 2020
Revised: April 21, 2020
Published online: May 27, 2020

[1] U. Leberle, http://www.cepi.org/taxonomy/term/14 (accessed: December 2019).
[2] R. Leblanc, https://www.thebalancesmb.com/paper-recycling-facts-figures-and-information-sources-2877868 (accessed: July 2018).

[3] Smithers, https://www.smithers.com/resources/2018/feb/paper-and-board-roles-in-the-future-of-packaging (accessed: February 2018).
[4] Ç. Koşak Söz, S. Trosien, M. Biesalski, *ACS Appl. Mater. Interfaces* **2018**, *10*, 37478.
[5] M. Wallmeier, E. Linvill, M. Hauptmann, J.-P. Majschak, S. Östlund, *Mech. Mater.* **2015**, *89*, 202.
[6] E. R. Alexey Vishtal, *BioResources* **2012**, *7*, 4424.
[7] M. Kuang, L. Wang, Y. Song, *Adv. Mater.* **2014**, *26*, 6950.
[8] M. Singh, H. M. Haverinen, P. Dhagat, G. E. Jabbour, *Adv. Mater.* **2010**, *22*, 673.
[9] S. Chen, M. Su, C. Zhang, M. Gao, B. Bao, Q. Yang, B. Su, Y. Song, *Adv. Mater.* **2015**, *27*, 3928.
[10] T. H. J. van Osch, J. Perelaer, A. W. M. de Laat, U. S. Schubert, *Adv. Mater.* **2008**, *20*, 343.
[11] F. Hoeng, J. Bras, E. Gicquel, G. Krosnicki, A. Denneulin, *RSC Adv.* **2017**, *7*, 15372.
[12] E. Sowade, F. Göthel, R. Zichner, R. R. Baumann, *Appl. Surf. Sci.* **2015**, *332*, 500.
[13] H. Saghlatoon, T. Björninen, L. Sydänheimo, M. M. Tentzeris, L. Ukkonen, *IEEE Antennas Wirel. Propag. Lett.* **2015**, *14*, 325.
[14] J. Hou, M. Liu, H. Zhang, Y. Song, X. Jiang, A. Yu, L. Jiang, B. Su, *J. Mater. Chem. A* **2017**, *5*, 13138.
[15] A. Albrecht, A. Rivadeneyra, A. Abdellah, P. Lugli, J. F. Salmerón, *J. Mater. Chem. C* **2016**, *4*, 3546.
[16] S. K. Tam, K. Y. Fung, G. S. H. Poon, K. M. Ng, *AIChE J.* **2016**, *62*, 2740.
[17] Y. Khan, F. J. Pavinatto, M. C. Lin, A. Liao, S. L. Swisher, K. Mann, V. Subramanian, M. M. Maharbiz, A. C. Arias, *Adv. Funct. Mater.* **2016**, *26*, 1004.
[18] P. Calvert, *Chem. Mater.* **2001**, *13*, 3299.
[19] G. Hu, J. Kang, L. W. T. Ng, X. Zhu, R. C. T. Howe, C. G. Jones, M. C. Hersam, T. Hasan, *Chem. Soc. Rev.* **2018**, *47*, 3265.
[20] J. Perelaer, B. J. de Gans, U. S. Schubert, *Adv. Mater.* **2006**, *18*, 2101.
[21] N. C. Raut, K. Al-Shamery, *J. Mater. Chem. C* **2018**, *6*, 1618.
[22] Y. Wang, H. Guo, J.-J. Chen, E. Sowade, Y. Wang, K. Liang, K. Marcus, R. R. Baumann, Z.-S. Feng, *ACS Appl. Mater. Interfaces* **2016**, *8*, 26112.
[23] E. Balliu, H. Andersson, M. Engholm, T. Öhlund, H.-E. Nilsson, H. Olin, *Sci. Rep.* **2018**, *8*, 10408.
[24] M. Tavakoli, M. H. Malakooti, H. Paisana, Y. Ohm, D. Green Marques, P. Alhais Lopes, A. P. Piedade, A. T. de Almeida, C. Majidi, *Adv. Mater.* **2018**, *30*, 1801852.
[25] Z. Zhang, T. Si, J. Liu, *Nanotechnology* **2018**, *29*, 415603.
[26] L. Shi, M. Layani, X. Cai, H. Zhao, S. Magdassi, M. Lan, *Sens. Actuators, B* **2018**, *256*, 938.
[27] L. Nayak, S. Mohanty, S. K. Nayak, A. Ramadoss, *J. Mater. Chem. C* **2019**, *7*, 8771.
[28] G. Largiller, D. Bouvard, C. P. Carry, A. Gabriel, J. Müller, T. Staab, *Mech. Mater.* **2012**, *53*, 123.
[29] Y. Akiyama, T. Sugiyama, H. Kawasaki, *Adv. Eng. Mater.* **2017**, *19*, 1700259.
[30] H.-J. Chan, B.-C. Huang, L.-W. Wang, K.-H. Liao, C.-Y. Lo, *Thin Solid Films* **2017**, *627*, 33.
[31] R. K. Holman, S. A. Uhland, M. J. Cima, E. Sachs, *J. Colloid Interface Sci.* **2002**, *247*, 266.
[32] R.-B. Song, K. Yan, Z.-Q. Lin, J. S. Chye Loo, L.-J. Pan, Q. Zhang, J.-R. Zhang, J.-J. Zhu, *J. Mater. Chem. A* **2016**, *4*, 14555.
[33] B. Reiser, L. González-García, I. Kanelidis, J. H. M. Maurer, T. Kraus, *Chem. Sci.* **2016**, *7*, 4190.
[34] P. Yang, L. Zhang, D. J. Kang, R. Strahl, T. Kraus, *Adv. Opt. Mater.* **2020**, *8*, 1901429.
[35] M.-C. Hsieh, C. Kim, M. Nogi, K. Suganuma, *Nanoscale* **2013**, *5*, 9289.
[36] R. Kattumenu, M. Rebros, M. Joyce, P. D. Fleming, G. Neelgund, *Nord. Pulp Pap. Res. J.* **2009**, *24*, 101.
[37] T. Öhlund, J. Örtegren, S. Forsberg, H.-E. Nilsson, *Appl. Surf. Sci.* **2012**, *259*, 731.
[38] K. Burek, F. Krause, M. Schwotzer, A. Nefedov, J. Süssmuth, T. Haubitz, M. U. Kumke, P. Thissen, *ACS Sustainable Chem. Eng.* **2018**, *6*, 14669.
[39] A. C. Siegel, S. T. Phillips, M. D. Dickey, N. Lu, Z. Suo, G. M. Whitesides, *Adv. Funct. Mater.* **2010**, *20*, 28.
[40] Q. Huang, W. Shen, Q. Xu, R. Tan, W. Song, *Mater. Chem. Phys.* **2014**, *147*, 550.
[41] H. Wu, S. W. Chiang, W. Lin, C. Yang, Z. Li, J. Liu, X. Cui, F. Kang, C. P. Wong, *Sci. Rep.* **2014**, *4*, 6275.
[42] C. Duan, X. Wen, C. Shi, Y. Zhao, B. Wen, Y. He, *J. Hazard. Mater.* **2009**, *166*, 478.
[43] A. K. Awasthi, X. Zeng, in *Waste Electrical and Electronic Equipment (WEEE) Handbook*, 2nd ed., (Eds: V. Goodship, A. Stevels, J. Huisman), Woodhead Publishing, Cambridge, UK **2019**, p. 311.
[44] A. Regattieri, M. Gamberi, M. Bortolini, F. Piana, *Sustainability* **2018**, *10*, 1587.
[45] C. Hagelüken, C. W. Corti, *Gold Bull.* **2010**, *43*, 209.
[46] W. Cheng, S. Dong, E. Wang, *Langmuir* **2003**, *19*, 9434.
[47] J. Blechschmidt, in *Paper Processing Technology* (Ed: J. Blechschmidt), Hanser Publications, Munich, Germany **2013**, p. 269.
[48] S. Wu, *J. Adhes.* **1973**, *5*, 39.